Current Biology, Volume *29*

Supplemental Information

Neandertal Introgression Sheds Light on Modern Human Endocranial Globularity

Philipp Gunz, Amanda K. Tilot, Katharina Wittfeld, Alexander Teumer, Chin Yang Shapland, Theo G.M. van Erp, Michael Dannemann, Benjamin Vernot, Simon Neubauer, Tulio Guadalupe, Guillén Fernández, Han G. Brunner, Wolfgang Enard, James Fallon, Norbert Hosten, Uwe Völker, Antonio Profico, Fabio Di Vincenzo, Giorgio Manzi, Janet Kelso, Beate St. Pourcain, Jean-Jacques Hublin, Barbara Franke, Svante Pääbo, Fabio Macciardi, Hans J. Grabe, and Simon E. Fisher

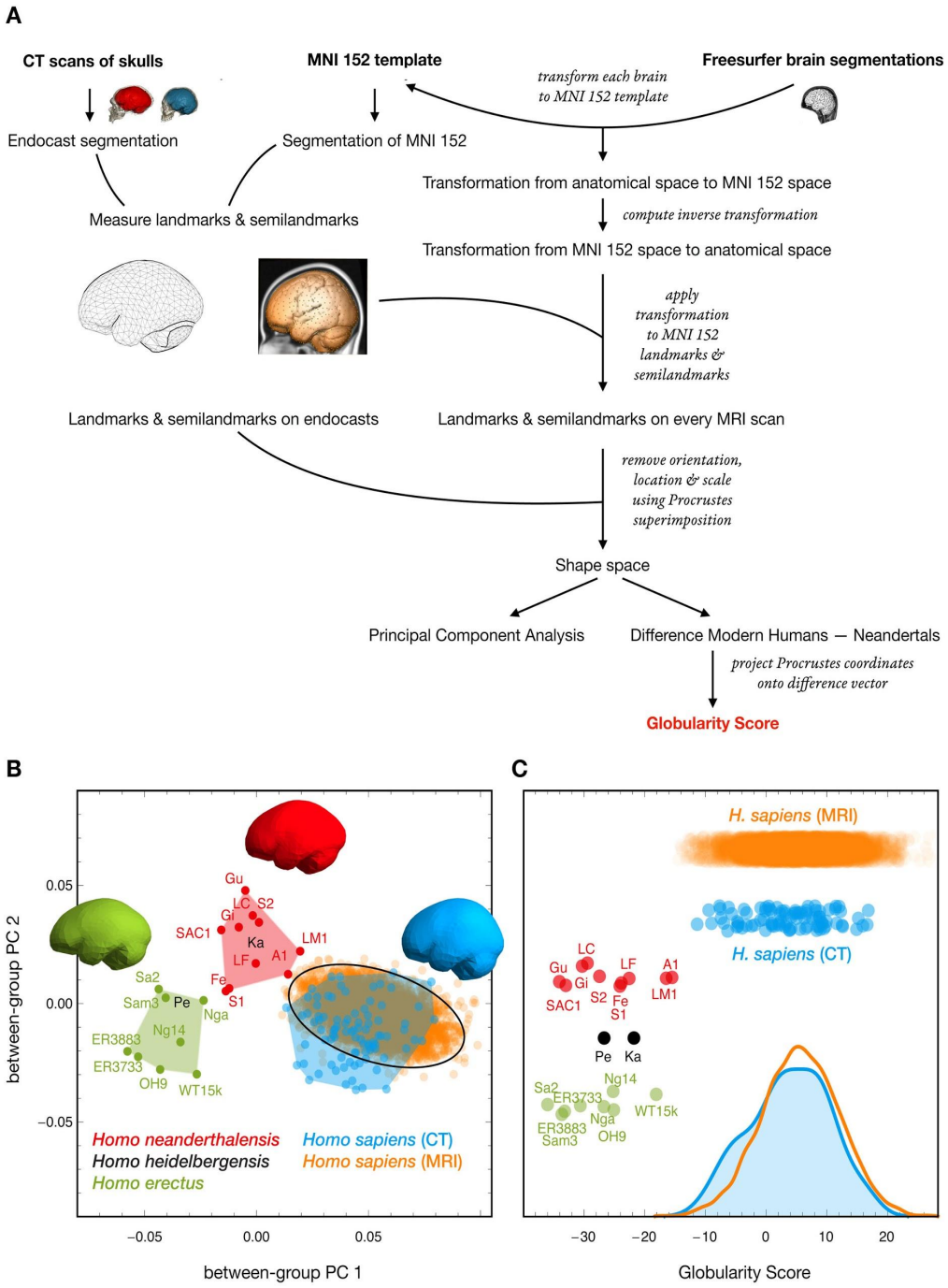

Figure S1. Globularity scores building on data published in [S1], Related to Figure 2. (**A**) Flowchart of the computations. (**B**) Between-group principal component (PC) analysis of endocranial shape: convex hulls are shown for modern human CT scans (blue; n=89), Neandertals (red; n=10), *Homo erectus* (green; n=8), and two *Homo heidelbergensis* individuals (black). Average endocranial shapes are shown in the respective group color. The between-group PCA scores of the MRI scans (orange) of living humans overlap with the modern human CT scans; the 99% confidence ellipse was computed for the MRI scans for which genetic data were also available (n=4,468). (**C**) Globularity score for each individual based on data in (B) plotted for each group separately; *Homo erectus*, *H. heidelbergensis*, and *H. neanderthalensis* have lower scores than contemporary *H. sapiens*. The frequency plots at the bottom show that the globularity scores of modern human CT scans and MRI scans overlap. As the sample composition of this dataset differs from the one shown in Figure 2, the values of the globularity scores also differ — the overall pattern, however, remains consistent.

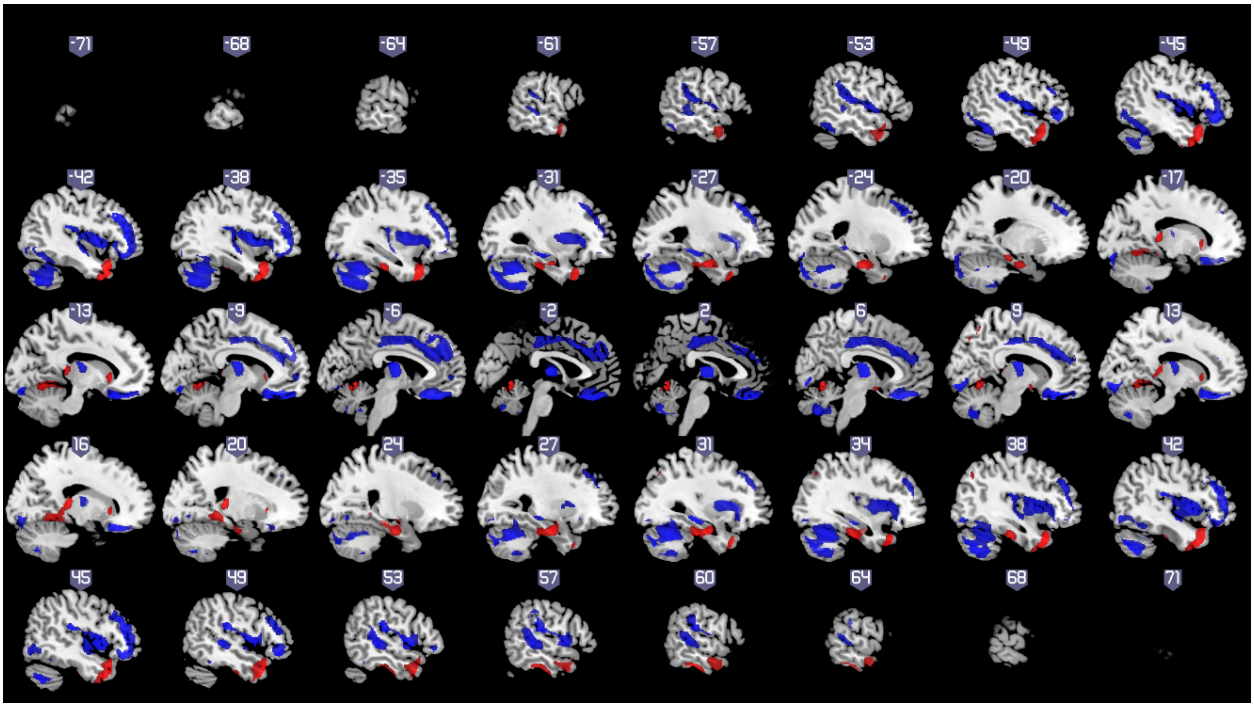

Figure S2. Voxel-based morphometry (VBM), Related to STAR Methods. VBM results of the gray matter (GM) analyses of variability in globularity in n=2,929 subjects. Significant clusters formed by voxels with FWE-corrected peak-level p<0.025 and with a cluster size ≥ 50 voxels are shown. VBM analyses were adjusted for age (modeled continuously using restricted cubic splines), sex, ICV, and cohort. Red: Significant positive associations between GM and globularity; blue: significant negative associations between GM and globularity. See also Tables S1 and S2.

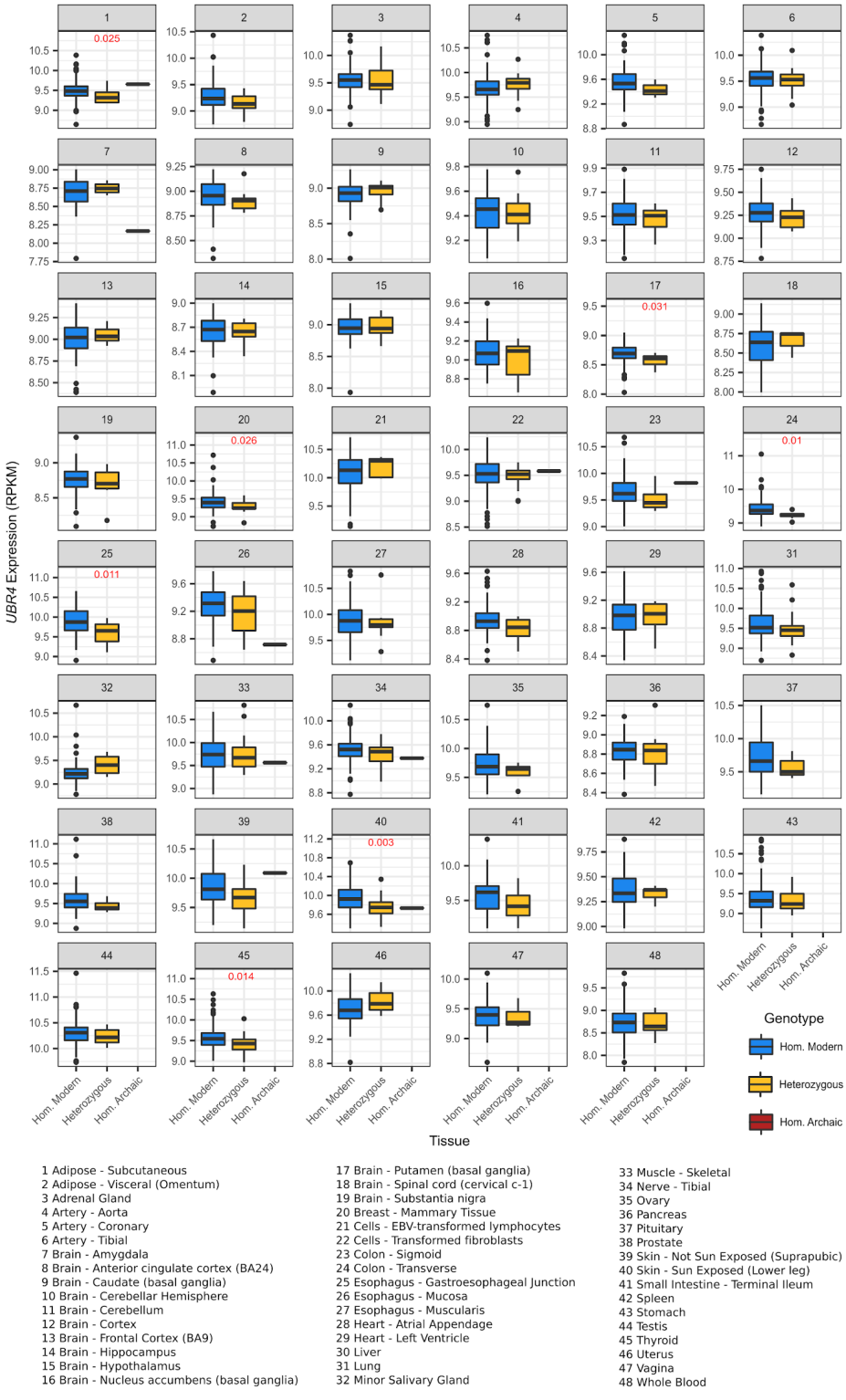

Figure S3. Gene expression *UBR4*, Related to Figure 4. Expression quantitative trait loci data from the GTEx resource, showing the impact of Neandertal alleles on gene expression for *UBR4*. Sample sizes are listed in Data S1.

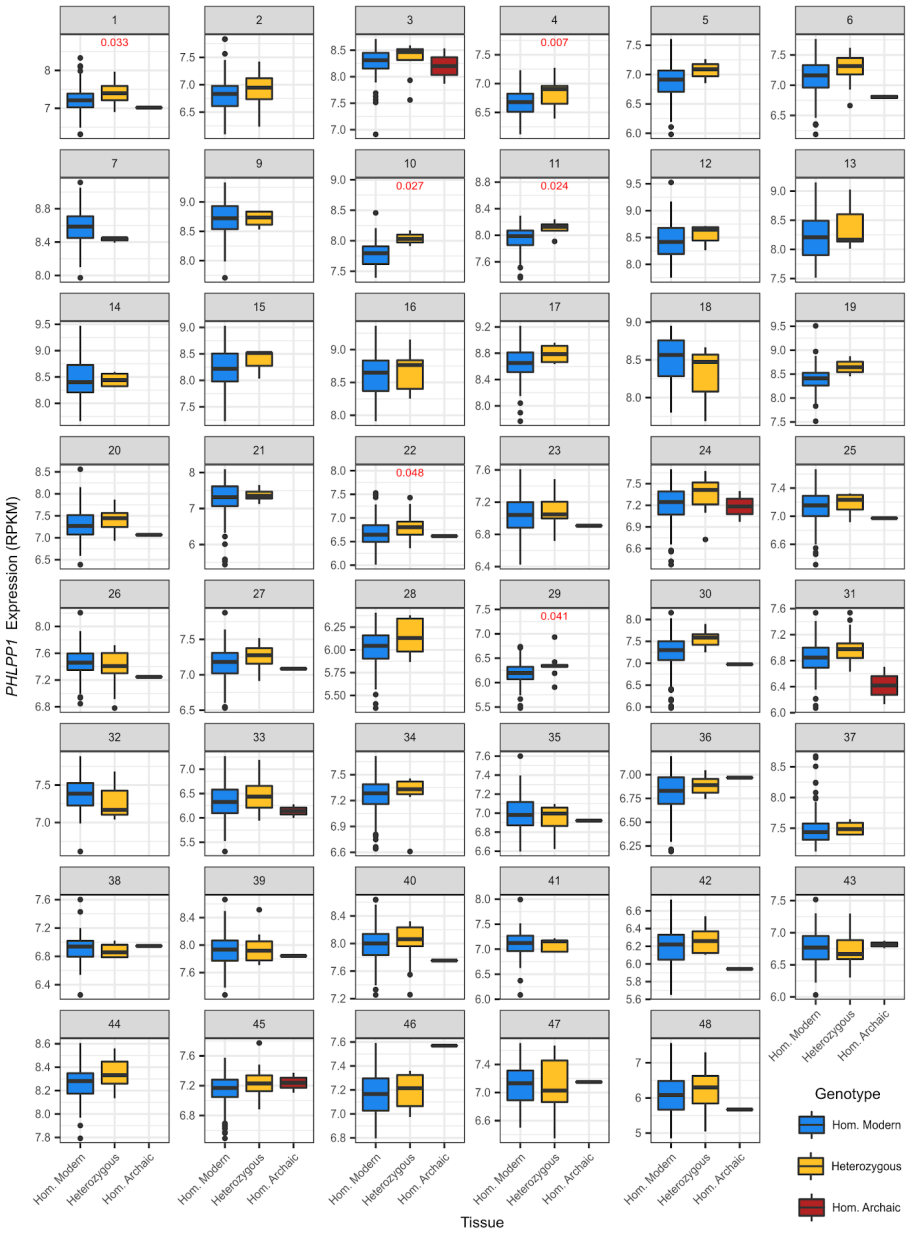

1 Adipose - Subcutaneous
2 Adipose - Visceral (Omentum)
3 Adrenal Gland
4 Artery - Aorta
5 Artery - Coronary
6 Artery - Tibial
7 Brain - Amygdala
8 Brain - Anterior cingulate cortex (BA24)
9 Brain - Caudate (basal ganglia)
10 Brain - Cerebellar Hemisphere
11 Brain - Cerebellum
12 Brain - Cortex
13 Brain - Frontal Cortex (BA9)
14 Brain - Hippocampus
15 Brain - Hypothalamus
16 Brain - Nucleus accumbens (basal ganglia)
17 Brain - Putamen (basal ganglia)
18 Brain - Spinal cord (cervical c-1)
19 Brain - Substantia nigra
20 Breast - Mammary Tissue
21 Cells - EBV-transformed lymphocytes
22 Cells - Transformed fibroblasts
23 Colon - Sigmoid
24 Colon - Transverse
25 Esophagus - Gastroesophageal Junction
26 Esophagus - Mucosa
27 Esophagus - Muscularis
28 Heart - Atrial Appendage
29 Heart - Left Ventricle
30 Liver
31 Lung
32 Minor Salivary Gland
33 Muscle - Skeletal
34 Nerve - Tibial
35 Ovary
36 Pancreas
37 Pituitary
38 Prostate
39 Skin - Not Sun Exposed (Suprapubic)
40 Skin - Sun Exposed (Lower leg)
41 Small Intestine - Terminal Ileum
42 Spleen
43 Stomach
44 Testis
45 Thyroid
46 Uterus
47 Vagina
48 Whole Blood

Figure S4. Gene expression *PHLPP1*, Related to Figure 4. Expression quantitative trait loci data from the GTEx resource, showing the impact of Neandertal alleles on gene expression for *PHLPP1*. Sample sizes are listed in Data S1.

Cluster size [voxel]	AAL-Regions	Brodman areas	$p_{peak, FWE}$	t score	Cohen's D	Stereotaxic coordinates [in mm] x	y	z
2264	L temporal pole (middle gyrus), L temporal pole (superior gyrus), L middle temporal gyrus, L inferior temporal gyrus, L fusiform gyrus	38, 21, 20, 47	$< 10^{-12}$ $2.50*10^{-5}$ 0.011	12.40 5.93 4.71	0.46 0.22 0.17	-38 -60 -50	21 0 -9	-36 -24 -44
3984	R parahippocampal gyrus, R inferior temporal gyrus, R fusiform gyrus, R lingual gyrus, R hippocampus, L lingual gyrus, R Cerebellum 4_5, R thalamus, Vermis_4_5, L Cerebellum 4_5, L Cerebellum 6, Vermis_6, L parahippocampal gyrus, R amygdala, R precuneus, R Cerebellum 6, L fusiform gyrus, L hippocampus	20, 19, 35, 36, 30, 28, 27, 34	$< 10^{-12}$ $< 10^{-12}$ $< 10^{-12}$	11.50 10.57 9.31	0.43 0.39 0.35	15 0 29	-33 -65 -12	11 -11 -26
2402	R temporal pole (middle gyrus), R middle temporal gyrus, R temporal pole (superior gyrus), R inferior temporal gyrus, R fusiform gyrus, R inferior frontal gyrus (orbital part)	38, 21, 20, 47	$< 10^{-12}$ $< 10^{-12}$ $5.77*10^{-6}$	11.44 10.34 6.18	0.42 0.38 0.23	39 45 65	23 15 -3	-36 -41 -21
180	L thalamus, L hippocampus	-	$< 10^{-12}$	9.96	0.37	-14	-35	9
879	L fusiform gyrus, L parahippocampal gyrus, L hippocampus, L amygdala, L Cerebellum 4_5, L inferior temporal gyrus, L Cerebellum 6	36, 35, 28, 20, 34	$2.39*10^{-12}$ $3.40*10^{-10}$	8.32 7.66	0.31 0.28	-27 -35	-12 -27	-26 -32
168	L caudate nucleus, L putamen	-	$1.12*10^{-11}$	8.12	0.30	-15	21	-2
118	R caudate nucleus, R putamen	-	$5.48*10^{-9}$	7.27	0.27	15	21	-2
58	R precuneus	7	$8.76*10^{-7}$ $1.41*10^{-5}$ $5.09*10^{-4}$	6.50 6.03 5.36	0.24 0.22 0.20	9 9 9	-72 -60 -63	47 60 53
71	L inferior temporal gyrus	34, 25	$9.81*10^{-6}$	6.09	0.23	8	2	-15
54	R angular gyrus, R superior occipital gyrus, R middle occipital gyrus	7, 19, 39	$8.26*10^{-4}$	5.26	0.20	32	-69	45

Table S1. Significant positive association of GM and Globularity, Related to STAR Methods. VBM results of the gray matter analyses on globularity in n=2929 subjects. Significant clusters formed by voxels with FWE-corrected peak-level p<0.025 and with a cluster size ≥ 50 voxels are provided. VBM analyses were adjusted for age (modeled continuously using restricted cubic splines), sex, ICV, and cohort. AAL-Regions and Brodman areas are listed according to the numbers of voxels they contribute to the respective cluster.

Cluster size [voxel]	AAL-Regions	Brodman areas	$p_{peak, FWE}$	t score	Cohen's D	Stereotaxic coordinates [in mm] x	y	z
1735	L thalamus, R thalamus	-	$< 10^{-12}$ $< 10^{-12}$ $< 10^{-12}$	13.24 11.20 10.65	0.49 0.41 0.39	0 -6 8	-12 -17 -15	9 18 18
5433	R Cerebellum 6, R Cerebellum Crus1, R Cerebellum Crus2, R Cerebellum 8, R fusiform gyrus, R lingual gyrus, R inferior occipital gyrus, R Cerebellum 7b, R inferior temporal gyrus, R middle temporal gyrus, R Cerebellum 4_5, R calcarine fissure (and surrounding cortex), R middle occipital gyrus	18, 37, 19, 17, 20	$< 10^{-12}$ $< 10^{-12}$ $< 10^{-12}$	11.21 9.60 9.31	0.42 0.36 0.35	42 5 30	-68 -81 -54	-44 -8 -30
3571	L gyrus rectus, R gyrus rectus, L superior frontal gyrus (orbital part), R superior frontal gyrus (orbital part), L medial orbital frontal gyrus, L inferior frontal gyrus (orbital part), R medial orbital frontal gyrus, R olfactory cortex, L olfactory cortex, R inferior frontal gyrus (orbital part), L middle frontal gyrus (orbital part)	11, 47, 25, 32	$< 10^{-12}$ $< 10^{-12}$ $< 10^{-12}$	10.80 10.38 9.32	0.40 0.38 0.35	-9 9 -2	24 26 45	-24 -24 -27
8609	R insula, R middle frontal gyrus, R Rolandic operculum, R inferior frontal gyrus (orbital part), R inferior frontal gyrus (triangular part), R putamen, R supramarginal gyrus, R superior temporal gyrus, R inferior frontal gyrus (opercular part), R superior frontal gyrus, R temporal pole (superior gyrus), R middle frontal gyrus (orbital part), R Heschl gyrus	13, 22, 40, 46, 47, 9, 10, 44, 43, 11, 6, 8, 21, 38, 45, 42, 2, 41	$< 10^{-12}$ $< 10^{-12}$ $< 10^{-12}$	10.35 10.20 9.51	0.38 0.38 0.35	48 42 44	-29 35 9	17 23 0
8433	L insula, L middle frontal gyrus, L superior temporal gyrus, L inferior frontal gyrus (triangular part), L Rolandic operculum, L inferior frontal gyrus (orbital part), L supramarginal gyrus, L superior frontal gyrus, L Heschl gyrus, L middle frontal gyrus (orbital part), L inferior frontal gyrus (opercular part), L putamen, L temporal pole (superior gyrus), L postcentral gyrus	13, 9, 22, 10, 47, 40, 8, 46, 41, 6, 11, 42, 43, 45, 21, 44	$< 10^{-12}$ $< 10^{-12}$ $< 10^{-12}$	10.03 9.47 9.22	0.37 0.35 0.34	-41 -44 -47	35 38 -32	21 -9 15
200	R hippocampus, R parahippocampal gyrus	-	$< 10^{-12}$	9.66	0.36	32	-23	-11
6641	L Cerebellum Crus1, L Cerebellum Crus2, L Cerebellum 6, L Cerebellum 8, L inferior temporal gyrus, L fusiform gyrus, L inferior occipital gyrus, L lingual gyrus, L Cerebellum 7b, L Cerebellum 9, L middle occipital gyrus, L Cerebellum 4_5, L calcarine fissure (and surrounding cortex)	37, 18, 20, 19, 36	$< 10^{-12}$ $< 10^{-12}$ $< 10^{-12}$	9.50 9.34 8.67	0.35 0.35 0.32	-9 -33 -39	-86 -54 -71	-14 -30 -42
5668	R middle cingulate cortex, L middle cingulate cortex, L medial superior frontal cortex, R anterior cingulate cortex, L anterior cingulate cortex, L supplementary motor area, R supplementary motor area, R medial superior frontal cortex, L superior frontal gyrus	32, 9, 24, 31, 8, 6, 10, 23	$7.37*10^{-12}$ $4.95*10^{-11}$ $1.59*10^{-10}$	8.17 7.92 7.77	0.30 0.29 0.29	-9 8 -8	33 -15 44	29 39 33
1226	R superior temporal gyrus, R middle temporal gyrus	22, 21, 13, 42	$2.72*10^{-11}$ $5.01*10^{-9}$	8.00 7.29	0.30 0.27	53 53	-35 -36	0 14
792	R Cerebellum 8, Vermis_8, R Cerebellum 9, L Cerebellum 8, Vermis_9, L Cerebellum 9, Vermis_7, L Cerebellum Crus2, R Cerebellum Crus2, L Cerebellum 7b	-	$5.39*10^{-11}$ $6.31*10^{-11}$ $4.10*10^{-10}$	7.91 7.89 7.64	0.29 0.29 0.28	6 18 -3	-66 -65 -66	-44 -45 -42
248	L hippocampus, L parahippocampal gyrus	27	$1.41*10^{-10}$	7.78	0.29	-30	-26	-11

53	R lingual gyrus, R fusiform gyrus	18, 19	$3.91*10^{-6}$	6.25	0.23	21	-72	-6
263	L middle temporal gyrus	22, 21	$2.23*10^{-4}$	5.52	0.20	-53	-35	5
			$1.96*10^{-3}$	5.09	0.19	-60	-30	-3
			$7.90*10^{-3}$	4.78	0.18	-56	-38	-5
92	L medial superior frontal cortex, L anterior cingulate cortex, L medial orbital frontal gyrus	10	$4.49*10^{-4}$	5.39	0.20	-11	54	0

Table S2. Significant negative association of GM and Globularity, Related to STAR Methods. VBM results of the gray matter analyses on globularity in n=2929 subjects. Significant clusters formed by voxels with FWE-corrected peak-level p<0.025 and with a cluster size ≥ 50 voxels are provided. VBM analyses were adjusted for age (modeled continuously using restricted cubic splines), sex, ICV, and cohort. AAL-Regions and Brodman areas are listed according to the numbers of voxels they contribute to the respective cluster.

	BIG†			SHIP-2			SHIP-TREND		
	n = 2433			*n* = 1139			*n* = 896		
	Est.	*p*	*Stat.*	*Est.*	*p*	*Stat.*	*Est.*	*p*	*Stat.*
Age	0.141	3.727 e-12	6.983	0.304	<2.2 e-16	10.766	0.296	<2.2 e-16	9.268
Sex	-0.0833	4.179 e-05	-4.105	-0.0027	0.9269	-0.092	0.0479	0.152	1.434
Intracranial volume	-0.0191	0.349	-0.936	0.0678	0.022	2.290	-0.0138	0.681	-0.412
Total white-matter	-0.0128	0.529	-0.630	0.0668	0.024	-2.257	-0.0234	0.485	-0.699
Total grey-matter	-0.0214	0.294	-1.0495	-0.0202	0.495	-0.683	-0.0939	0.005	-2.818
Cerebellar volume	-0.0823	5.255 e-05	-4.0513	-0.0095	0.749	-0.321	-0.0908	0.007	-2.725
Depression				-0.0197	0.54	-0.613	-0.0419	0.211	-1.252
Tobacco Use (current)				0.0156	0.629	0.483	-0.0433	0.197	-1.292
Tobacco Use (ever)				-0.0328	0.308	-1.0192	-0.0426	0.204	-1.272

Table S3. Correlations between endocranial globularity and demographic or MRI-derived variables, Related to STAR Methods. Variables in *italics* are controlled for the effect of age. † Variables in the BIG cohort were also controlled for sex and differing scanner parameters.

Supplemental References

S1. Neubauer, S., Hublin, J.J., Gunz, P. (2018). The evolution of modern human brain shape. Sci Adv 4, eaao5961.